Mon. Not. R. astr. Soc. (1972) **157**, 419–431.

OBSERVATIONS OF THE SUPERNOVA REMNANT IC443 AT 1·42 GHz

I. E. Hill

(Received 1972 January 21)

SUMMARY

The supernova remnant IC443 has been mapped at 1·42 GHz with a resolution of 1′·05 × 2′·71 arc, using the Half-Mile telescope at Cambridge. The map shows that the source has a thick shell extending over the eastern half of its circumference with no evidence of a shell on the western edge. There is remarkably detailed agreement of optical and radio features, with some optical filaments clearly located on the outer edge of radio ridges. Comparison of the map with other high resolution maps at higher frequencies shows an increase in the spectral index near the brightest optical features. Estimates of some physical parameters of the source are derived in the final section of the paper.

1. INTRODUCTION

The supernova remnant IC443, at $l = 189°$, $b = +3°{\cdot}2$, is visible optically as an irregular shell of nebulosity about 45′ arc in diameter and brightest towards the neighbouring nebula, Sharpless 249, in the north-east. The distance of IC443 is generally assumed to be that of S249, 1·5 kpc (Sharpless 1965), and its age is about 60 000 years (Minkowski 1971).

At radio wavelengths IC443 shows shell structure more or less coincident with the optical nebulosity and still partially unresolved with beams as small as 4′ arc (Dickel 1971; Milne 1971). The integrated spectral-index α is 0·45 (where $S \propto \nu^{-\alpha}$), which implies that most of the radiation is non-thermal and presumably due to synchrotron emission. This is confirmed by the detection of linear polarization at wavelengths shorter than 6 cm (Kundu & Velusamy 1969; Dickel 1971; Milne 1971), indicating a magnetic field which is radial over the southern rim of the nebula, but randomly oriented near the brighter north-eastern rim. Milne (1971) has recently suggested that there is a detectable thermal component of the radiation from the area of the brightest optical features.

This paper presents a high-resolution map of IC443 obtained at 1421 MHz by means of aperture synthesis with the Half-Mile telescope at the Mullard Radio Astronomy Observatory. The observations are described in Section 2 and the results in Section 3. These are discussed in Section 4.

2. OBSERVATIONS

The Half-Mile telescope described by Baldwin *et al.* (1970) records three interferometer responses which yield, by Fourier inversion, maps of the combinations $I+U$, $I-U$, and Q of the Stokes parameters representing the polarized brightness distribution of the source, if it is assumed that the circular polarization $V = 0$.

During January and February 1971, 12-hr observations of an area of sky approximately $2° \times 2°$ centred on the point $\alpha = 06^h\,14^m\,0^s{\cdot}0$, $\delta = 22°\,42'\,40''$ (1950·0) were made at each of 45 aerial spacings. Adjacent spacings were separated by 12·2 m and the minimum spacing was also 12·2 m. The synthesized beam has a half power width of $1'{\cdot}05$ arc in right ascension and $2'{\cdot}7$ arc in declination, with a first side-lobe response of 5 per cent. The lack of spacings smaller than 12·2 m places an upper limit of $30' \times 75'$ on the angular diameter of the structure which is accurately represented on the map. Larger features are progressively less well represented. Since the first grating response has radii of $1° \times 2°{\cdot}7$, only low surface brightness features have grating responses in the area shown in Fig. 1, and these do not affect the map significantly.

Daily observations of the unresolved sources 3C 287 and 3C 409 were used to calibrate the telescope. Their assumed positions (1950·0) and flux densities were

3C 287	$\alpha = 13^h\,28^m\,15^s{\cdot}69$	3C 409	$\alpha = 20^h\,12^m\,18^s{\cdot}01$
	$\delta = 25°\,24'\,36''{\cdot}8$		$\delta = 23°\,25'\,45''{\cdot}0$
	$S = 6{\cdot}9$ f.u.*		$S = 13{\cdot}9$ f.u.

and all the maps are in 1950·0 coordinates.

3. RESULTS

3.1. *General*

The *I* map of total brightness is shown in Fig. 1. Note that the apparent faint extensions of the source near $\alpha = 06^h\,14^m\,30^s$, $\delta = 23°\,00'$ and $\alpha = 06^h\,13^m\,30^s$, $\delta = 22°\,00'$ are not real, but are due to partial obscuration of one of the dishes by the other at extreme hour angles at the shortest spacing. The unresolved source (4C 22·14) at $\alpha = 06^h\,12^m\,32^s{\cdot}9$, $\delta = 22°\,42'\,35''$ is probably an unrelated background object. Its flux density from this map is $S_{1420} = 0{\cdot}55$ f.u. and the 4C flux is $S_{178} = 2{\cdot}3$ f.u., giving it a spectral index $\alpha = 0{\cdot}69 \pm 0{\cdot}02$. The source does not appear in any other survey at radio frequencies. The optical field on the Palomar Sky Survey prints is partially obscured by the nebula, but shows a cluster of stars at the position of the source with no galaxies visible in the vicinity. Sidelobes are responsible for the distortion of the contours near this object.

The total flux density of IC443 was determined both by integration of the map and by extrapolation to zero spacing of the visibility function, giving values of $S_{1420} = 138 \pm 15$ f.u. and $S_{1420} = 190 \pm 30$ f.u. respectively. A uniform brightness distribution with the diameter of the nebula is not quite mapped correctly in α with the incremental spacing used, so the former value represents a lower limit to the flux density from IC443. On the other hand, the latter value includes a contribution from the extended component associated with S249, a component explicitly excluded from the former value. Hogg (1964) obtained values of 170 ± 20 f.u. and 40 ± 20 f.u. as the 1·4 GHz fluxes from IC443 and the extended component respectively, and Milne & Hill (1969) determined the flux from IC443 alone as 131 ± 13 f.u. at this frequency.

* 1 f.u. = 10^{-26} W m^{-2} Hz^{-1}.

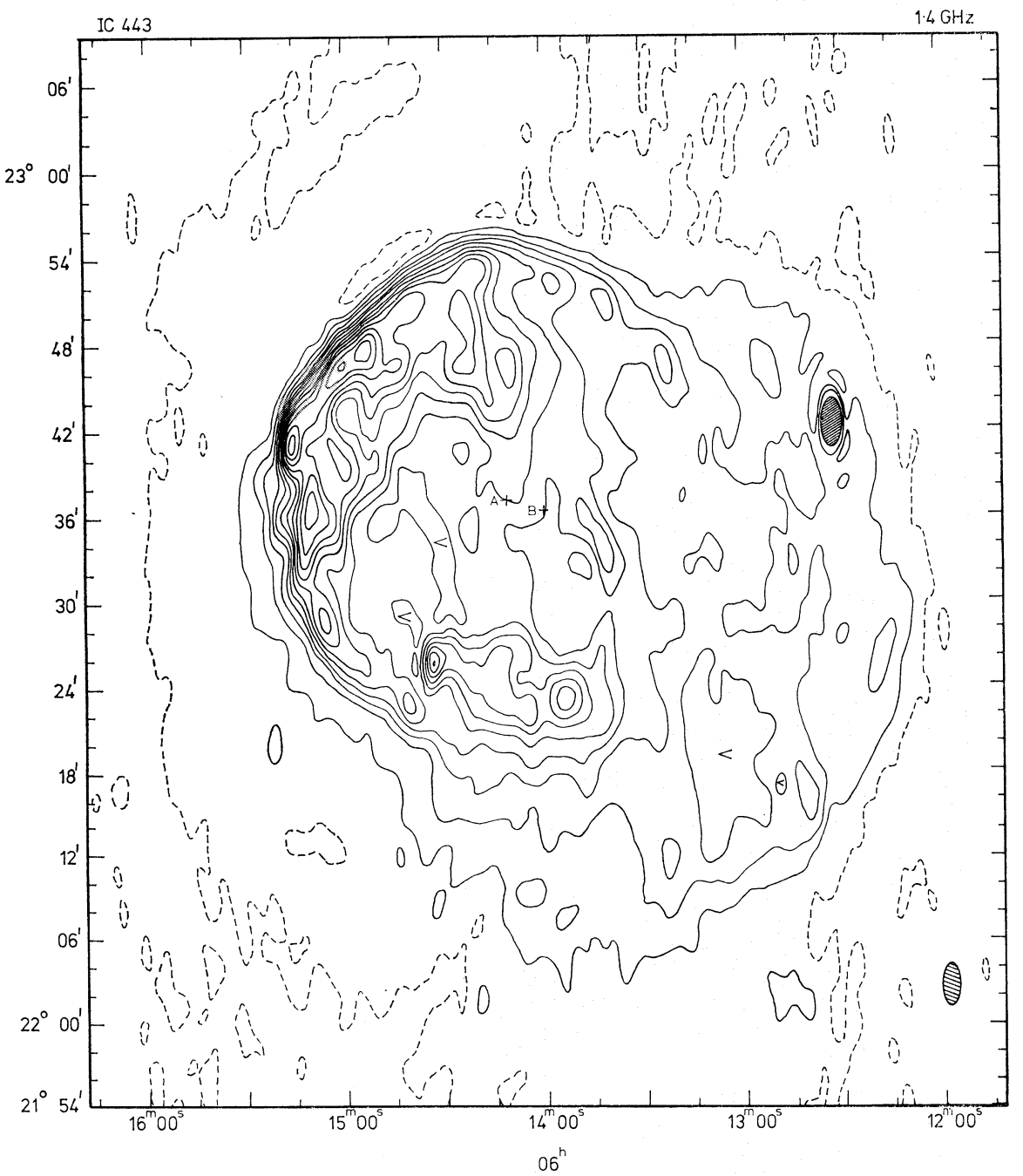

FIG. 1. *Total intensity isotherms at 1·42 GHz. The contour interval is 4 °K in brightness temperature and the dotted contour is 1 °K above the arbitrary zero level. Isolated minima are marked with the symbol <. The beam at half power is shown by the shaded ellipse and the r.m.s. noise level at the map centre is 0·5 °K.*

Although the Stokes parameters Q and U were recorded, the degree of polarization is less than 3 per cent and was too low for useful polarization maps to be made.

3.2. *The radio shell structure*

The bright north-eastern region of the source consists of a continuous narrow ridge with a sharp outer edge which is unresolved over most of its length, even

where the effective beam width is 1′ arc. The inner edge, on the other hand, is poorly defined and is characterized by resolved structure extending inwards. The ridge, with its irregular peaks, presumably represents the projection of a shell of emission. The bright southern area could be regarded as an extension of this shell but its outer edge is resolved. The western part of the source shows no shell structure.

The most striking feature of the radio shell is its near circular outline around half the circumference of the source. A circle centred at A (Fig. 1, $\alpha = 06^h\ 14^m\ 11^s$, $\delta = 22°\ 37'{\cdot}5$) and having a radius of 15′ arc passes through eight of the 11 isolated peaks on the eastern and northern edges of the source, and lies along the outer edge of the bright southern peak. Although this circle is a good fit over a large part of the radio shell, it is very different from the outline of the optical nebulosity, and is not the best fit to the brightest part of the shell. The apparent circularity of the shell is partly due to the elongated beamshape, which makes the ridge of the shell closer to the edge of the source on the eastern boundary than on the northern boundary, thereby reducing the apparent radius of the shell. This effect was confirmed by comparison of the circle with the map after the latter had been convolved to a circular beamshape with 3′ arc half-power width. A circle of larger radius, with centre at B ($\alpha = 06^h\ 14^m\ 00^s$, $\delta = 22°\ 36'{\cdot}8$), coincides with both radio and optical boundaries of the brightest part of the object and is a reasonable fit to all except the southern and north-western parts of the shell.

An estimate of the shell thickness can be obtained by comparison of the observed radial profile with that predicted by a uniform spherical shell model consisting of a shell of thickness ΔR and outer radius R, which radiates isotropically. Rosenberg (1970) has applied such a model to Cas A. As the optical emission comes from near and far sides of the shell (Lozinskaya 1969) and the radio and optical emission are closely related (Section 3.3) it is reasonable to assume that the shell is complete over the area of the optical shell. The shell is obviously not uniform but a mean radial profile can be obtained by integration over a large sector of the source. Deviations of the shell from circularity place an upper limit on the size of sector that may be used. Mean radial profiles (Fig. 2) were derived for the sectors of the source between position angles $-10°$ and 100° and between 45° and 80°. The map, smoothed with a circular beamshape, was divided into a series of rings 2′ arc wide and concentric about the point B, and the mean brightness determined for each ring in both of these sectors. The narrower sector was chosen to avoid irregularities in the outline of the shell and the exceptionally bright area inside the shell near the north of the source. This area is brighter than much of the radio shell and would be 2 to 3 times brighter still if it were viewed edge on as part of the same spherical shell. A model-fitting procedure was used to find the values of R and ΔR for the uniform spherical shell which gives radial profiles, as smoothed with a 3′ arc beam, agreeing best with the observed profiles. These model profiles are shown as the smooth curves in Fig. 2 and the optimum values are $R = 20'$ arc, with $\Delta R = 5'{\cdot}3$ arc for the larger sector and $\Delta R = 3'{\cdot}4$ for the smaller. The model gives a better fit to the mean profile from the narrower sector and the lower value of ΔR will be used as the shell thickness. For the larger sector the model predicts a peak brightness at a smaller radius than is observed, possibly as a result of the bright area described above which increases the central brightness considerably.

Although a thick shell gives a reasonable fit to the mean profiles, its outer

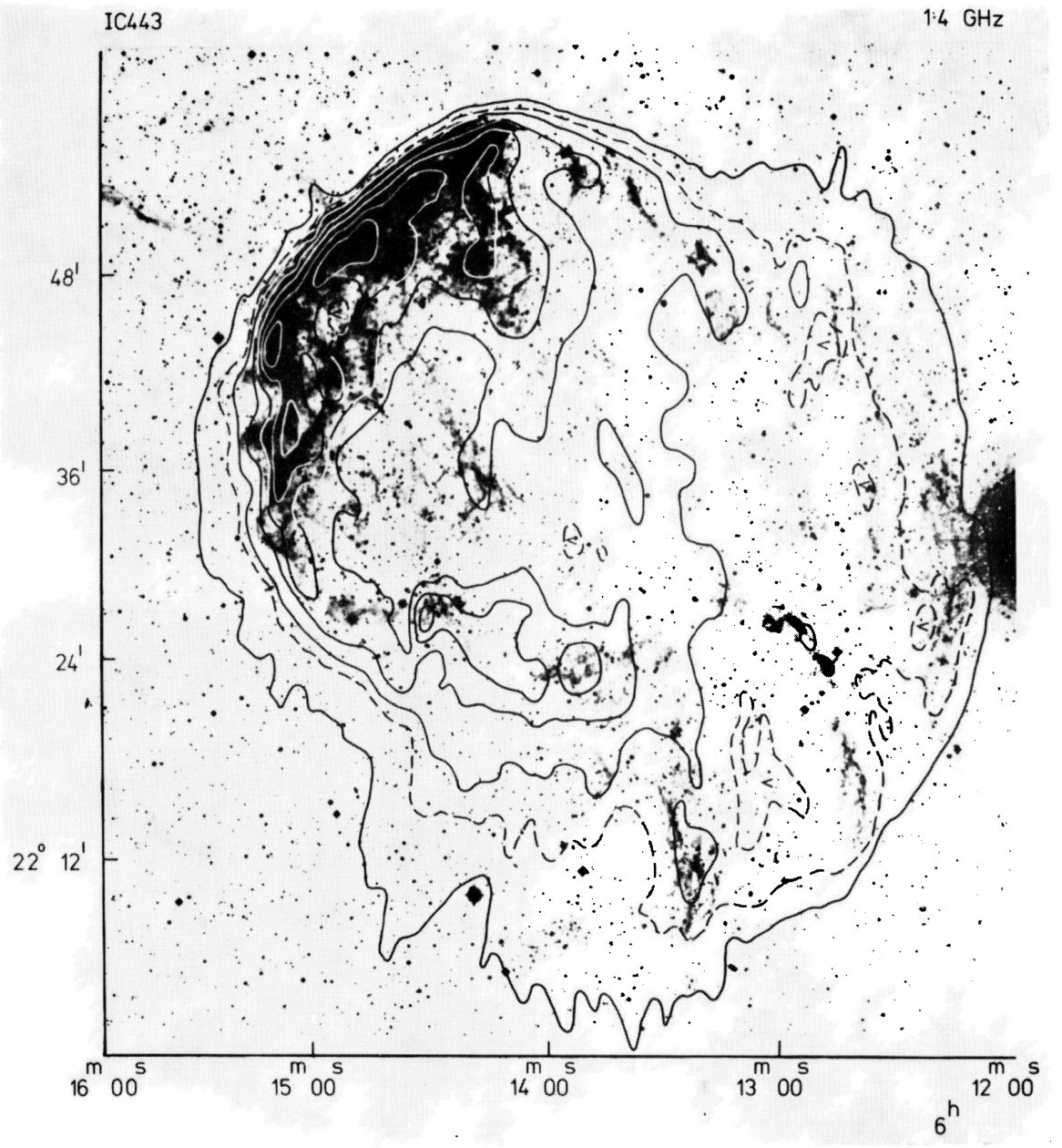

PLATE I. *The map of Fig.* 1 *superimposed on the optical field from the red print of the National Geographic Society–Palomar Sky Survey. The contour interval is* 8 °*K in brightness temperature and the dotted contour is midway between adjacent contours. The zero level is* 4 °*K below the first contour. Isolated minima are marked with the symbol* <.

[*facing page* 422]

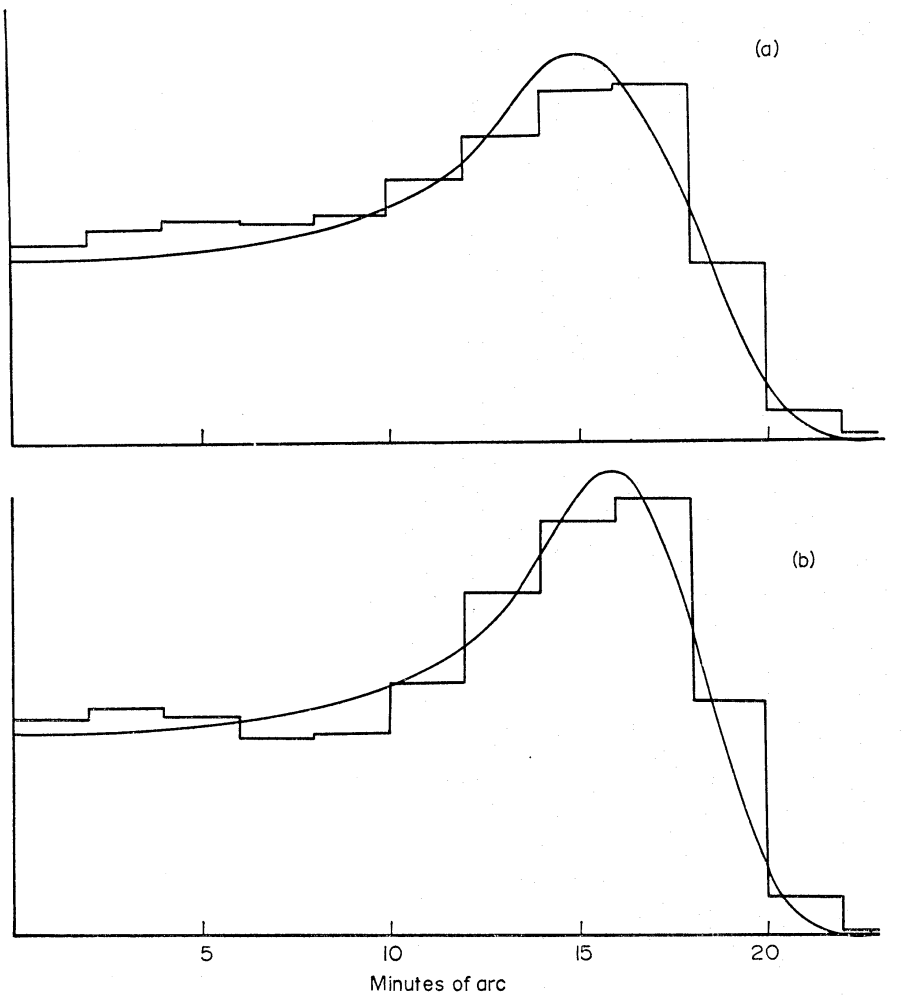

FIG. 2. (a) *The histogram is the mean radial profile for the sector of the shell between position angles* −10° *and* 100°. *The smooth curve is the best fit achievable with a uniform shell model radiating isotropically. The vertical scale is in arbitrary units.* (b) *The mean radial profile and best-fit model for the sector of shell between position angles* 45° *and* 85°.

edge would be resolved by a 1′ beamwidth. The shell shows some features as narrow as 1′ arc superimposed on the broader ridge which has been assumed to represent the shell. If the shell were less than 1′ arc thick and very irregular it could appear to be a thick shell when unresolved, but such a model could not account for the high central brightness of the source. A combination of thick and thin shells, or a shell with an emissivity that decreased sharply from the outside to the inside edge, could give a thick ridge with unresolved structure on its outer edge and so be consistent with the central brightness.

3.3. *Comparison with optical photographs*

In Plate I the map from Fig. 1 is superimposed on a reproduction of the optical field taken from the red print of the National Geographic Society–Palomar Sky Survey. The projection in declination of the radio map is not identical to that of the photograph, but the difference is sufficiently small for large parts of the map to be correctly aligned with the optical field. In Plate I, the north-eastern area is correctly aligned and the error in the southern part of the source is less

than 40″. In the discussion that follows, comparisons between optical and radio features are made with the photograph and the map correctly aligned for the area under consideration.

The degree of correlation of optical and radio features is remarkable, particularly in the low surface brightness parts of the source. The correspondence of the brightest region of the radio source with the brightest nebulosity is well known, but a much more detailed association of optical and radio features is shown by these observations. There is an overall agreement of radio peaks with optical features, to the extent that each radio peak or ridge coincides with an optical feature, and more extended radio structure covers the same area as the more diffuse optical emission. The outlines of the radio and optical objects are very similar, as is illustrated by the 'bays' in both radio and optical outline at $\alpha = 06^h\ 15^m\ 20^s$, $\delta = 22°\ 38'$ and $\alpha = 06^h\ 15^m\ 15^s$, $\delta = 22°\ 33'$, and by the low brightness plateaux bordering the source in the SE and NW quadrants. These plateaux have optical counterparts, although these are not readily visible on Plate I.

A more detailed comparison of the positions of peak radio brightness relative to the optical filaments is of some interest. Along the NE edge of the nebula, the peak of the radio shell lies 2′–3′ inside the outer rim of the nebula, but the outermost radio contour includes all the optical emission. This suggests that the outer boundary of the radio source is either slightly behind, or coincident with, the optical boundary but higher resolution maps are required to confirm this. The south-western part of the nebula has three prominent ridges of optical radiation, all of which have radio components as is shown in Fig. 3. The two regions furthest to the west have unresolved outer edges with a region of enhanced emission extending behind them, whereas the third, at both radio and visible wavelengths, has a central emission ridge with extended structure on both sides.

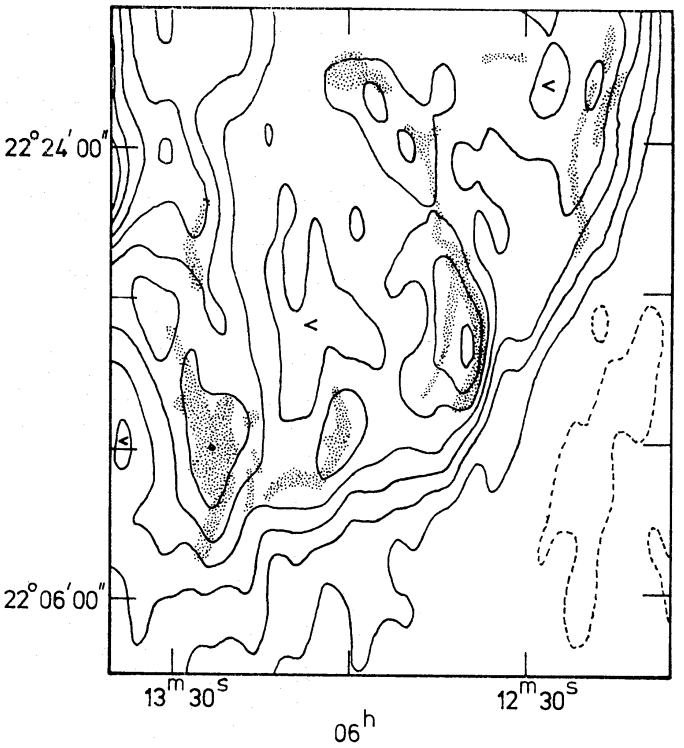

FIG. 3. *The south-western part of the supernova remnant with the brighter optical features shaded in. The contour interval is 2 °K.*

The half-power contours of the unresolved edges of the former two features lie approximately along the outer edge of the filaments, as seen in Fig. 3. A possible explanation of such structure is given in Section 4. High resolution observations of the Cygnus Loop (Moffat 1971) show a similar relationship between optical and radio maps.

Most radio maps of IC443 reveal an extended component associated with the H II region S249. As was discussed in Section 2, it is unlikely that this feature would be visible on the present map but any small scale structure in the parts of S249 nearest IC443 should be detectable. The broad plateau visible to the east of the source and above the background level to the west of the source is the only indication of the extended component, but its outer contour is almost certainly not real. Some narrow features are visible near the filaments at $\delta = 22^\circ\,50'$, and on the map smoothed with a 3′ arc circular beam there is a ridge 9′ arc wide, bounded by the bright filament and 1·5 °K brighter than the local background.

3.4. *Thermal component*

Milne (1971) has recently suggested that there may be an appreciable free–free contribution to the radio emission from the optically brighter parts of IC443 if an electron temperature of 10^4 °K and an Hα flux of $1{\cdot}3 \times 10^{-8}$ erg cm^{-2} s^{-1} (Hogg 1964) is assumed, and if the nebula is collisionally excited. A comparison of his map at 5 GHz and that of Hogg (1964) at 1·4 GHz showed a displacement of the peak spectral index from the optical shell and a flattening of the spectrum at the north-eastern edge of the nebula possibly due to such a component. This comparison was limited by the 10′ arc resolution of Hogg's observations but the map in Fig. 1 has now been used to provide a spectral index distribution with the higher resolution of Milne's 4′ arc beam. The map was convolved to a circular gaussian beamshape similar to Milne's and compared, point by point, with the 5 GHz map to give the distribution of temperature spectral index, β (where $T \propto \nu^{-\beta}$), shown in Fig. 4. The largest errors in β occur in the low brightness areas of the source where the uncertainty in the 1·4 GHz zero level is more serious and also, as a result of the techniques used in digitizing the 5 GHz map, near unresolved edges on this map. Over most of the source, however, the uncertainty in the *relative* values of β is less than $\pm 0{\cdot}1$. The *absolute* values of β are considerably less reliable since systematic errors of less than 10 per cent in the temperature scales of the maps would change the spectral index by about 0·1 at each point without changing the relative values of β. The contours in Fig. 5 are terminated either at the lowest contour of the 5 GHz map, or where the brightness at 1·4 GHz is less than 3 per cent of the peak brightness, the more stringent condition being applied at each point. A second spectral index map was constructed from the 1·4 GHz map and that of Dickel (1971) at 6·6 GHz with a resolution of 4′·2 arc. The difference between the spectral indices found from these two pairs of maps is less than $\pm 0{\cdot}1$ over a large part of the source although the 1·4–6·6 GHz spectral indices are lower on average than the 1·4–5·0 GHz values. The dotted contours in Fig. 5 represent those areas where the difference between the spectral indices exceeds $\pm 0{\cdot}2$.

Both spectral index maps show variations in β over the source but the only large scale feature common to both is a region, roughly coincident with the brightest part of the optical shell, where the 1·4–5·0 GHz spectral index is greater

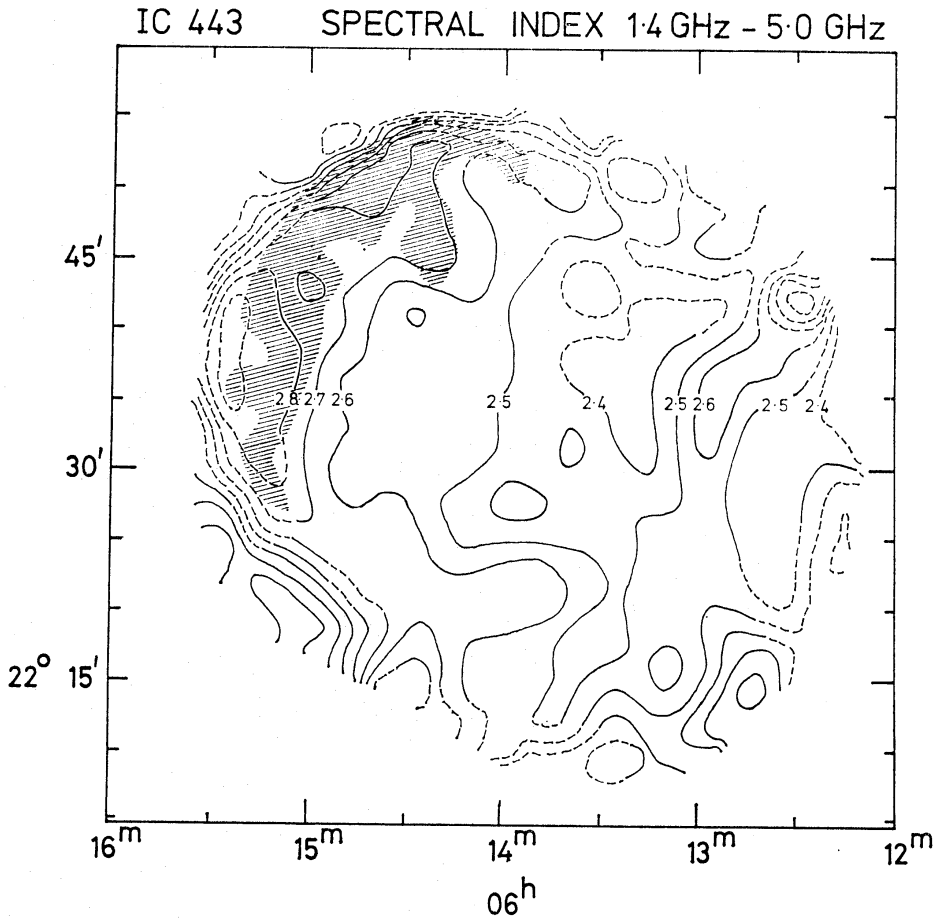

FIG. 4. *The distribution of temperature spectral index, β, derived from the map presented here and that of Milne at 5·0 GHz. The position of the north-eastern optical shell is represented by the shaded area. The dashed contours are explained in Section* 3.4.

than 2·6 and, in places, as high as 2·8. The outer boundary of this area of high spectral index apparently coincides with the edge of the optical and radio shells, and its highest values lie near the peak of radio brightness, although these apparent positional correlations must be regarded with caution because of the large errors at the edge of the source. The relative errors in the spectral indices for the bright parts of the shell are ±0·04 while for the central and western parts of the source the errors are larger and are dominated by the uncertainty in the zero level of the 1·4 GHz map. Nevertheless, the difference between the spectral indices of the central and eastern parts of the source cannot be attributed to an extended background not represented in Fig. 1. Comparison of this map with that of Hogg (1964) shows that an extended background of about 1·5 °K underlies the adopted zero level, whereas an extended background greater than 5 °K would be required to remove the difference in spectral index. The displacement, reported by Milne (1971), of the peak spectral index from the optical shell could be due to a resolution effect. The same effect would explain Hogg's (1964) conclusion that the peak radio brightness is similarly displaced from the shell. Kundu & Velusamy (1968) have reported a curved spectrum for this region with $\beta = 2{\cdot}35$ in this frequency range and an even flatter spectrum at lower frequencies, but their resolution was lower still. Changes in the spectral index across the source have been found in

the supernova remnants HB21 (Erkes & Dickel 1969) and W49B (Wynn-Williams 1969), but both of these sources have flatter spectra associated with the component brighter at 1·4 GHz in contrast with the steeper spectrum found here.

The steeper radio spectrum in the vicinity of the optical shell implies that free–free emission is not the dominant origin of radiation from this part of the source, but that the electron spectrum is correspondingly steeper. This will be discussed further in Section 4.

4. DISCUSSION

4.1. *General*

The previous section has shown that the radio source associated with IC443 has a thick shell (about one-sixth of the radius), with smaller scale structure embedded in it and with optical filaments on the outer edge. The shell extends over only half of the circumference although the other half does have several ridges also with optical filaments on their leading edges. The central brightness is comparatively high for a shell source. It is interesting to compare it with the Cygnus Loop, the old supernova remnant which has been studied in most detail (Moffat 1971). The latter source has a thin shell (about one eighteenth of the radius) with a very low central brightness; it also shows a close association of optical and radio emission although the brightest radio and optical features are not, in fact, coincident. The radius of the Cygnus Loop shell is 20 pc compared with 8·2 pc for IC443, both objects are remnants of type II supernova outbursts, and they have nearly the same age (Minkowski 1968). The expansion velocity of the Cygnus Loop is 100 km s^{-1} and that of IC443 is 65 km s^{-1} (Lozinskaya 1969). In the discussion that follows, an attempt will be made to explain the differences between the sources.

4.2. *Expansion of the shell*

Three distinct phases in the expansion of a supernova remnant can be identified. These are the initial expansion, which is essentially free and determined only by the initial conditions, an adiabatic phase best described by a blast-wave solution (Sedov 1959), and finally a momentum-conserving phase. During the adiabatic phase the energy of the expanding remnant as a function of radius and velocity is (Sedov 1959),

$$\mathscr{E} = 7{\cdot}7 \times 10^{41} N_0 R^3 V^2 \text{ erg} \qquad (1)$$

where N_0 is the interstellar particle density in cm^{-3}, R is the radius of the shell in parsec and V the velocity of expansion. The momentum-conserving phase is entered when the radiative loss rate is comparable with the rate of conversion of kinetic energy to thermal energy in the shell. The final momentum of the shell depends on the radiative loss rate, the interstellar density and the initial energy of the outburst, and has been estimated by Poveda & Woltjer (1968), Cox (1970) and Woltjer (1970), all of whom obtain similar values. Woltjer gives the following expression for the initial energy of the shell if it is already in the momentum-conserving phase,

$$\mathscr{E} = 2 \times 10^{44} (R^3 V)^{17/16} N_0^{19/16} \qquad (2)$$

which is essentially his equation (14). It is not obvious which phase of expansion IC443 has reached, but Moffat's (1971) observations of the Cygnus Loop are consistent with a momentum-conserving model for its expansion. Since both the radius and the expansion velocity of IC443 are smaller than those of the Cygnus Loop, the former must either be the remnant of a less energetic supernova, or the expanding shell must have been decelerated more rapidly by the interstellar medium. If it is assumed that the Cygnus Loop has a momentum-conserving shell and that both supernovae had the same initial energy, the interstellar density near IC443 must be at least an order of magnitude greater than that near the Cygnus Loop. It is more likely, however, that differences in both the initial energy and the interstellar density contribute to the observed differences between the remnants.

The present radius of the north-eastern shell is 8·2 pc for a distance of 1·5 kpc and the expansion velocity is 65 km s^{-1}. For a typical interstellar density of 1 cm^{-3} these values give initial energies of 2×10^{48} erg if the shell is still in the blast-wave phase or 10^{49} erg if the shell is momentum-conserving. Estimates of the kinetic energy of Cas A, which shows some of the features of a type II supernova, give 10^{51} erg (Minkowski 1968), but Poveda (1964) obtained a value of 5×10^{49} erg for type II remnants from kinetic energy arguments. Equation (1) gives 10^{51} erg for the energy of Tycho's supernova of type I (Minkowski 1968). Woltjer found $\mathscr{E} = 4 \times 10^{49}$ erg from equation (2) for the Cygnus Loop on the assumption that $N_0 = 0{\cdot}3$ cm^{-3}, but Moffat (1971) has suggested that N_0 could be as high as 5 cm^{-3} in parts. The higher density would imply an initial energy larger by an order of magnitude. These estimates imply that IC443 had a low initial energy, particularly if it is still in the blast-wave stage of expansion, and provided that the interstellar density is $\simeq 1$ cm^3 in its vicinity. There are indications, however, that IC443 is expanding into a region of high density. Twenty-one cm line observations, for instance, show a cloud of neutral hydrogen ahead of the north-eastern part of the shell with density of 10–20 cm^{-3} (Locke, Galt & Costain 1964; Akabane 1966). A density of 10 cm^{-3} gives energies of 2×10^{50} erg for adiabatic and momentum-conserving expansions respectively. These energies are more nearly in agreement with other estimates of the initial energy of a type II supernova and the high density ahead of the shell is confirmed by consideration of the physical conditions in the shell as discussed in Section 4.3.

The difference between the radii of the eastern and western halves of the remnant can be explained by a density gradient in the interstellar medium. Since $R \propto (1/N_0)^{1/5}$ during the blast-wave phase of expansion the ratio of radii ($R_w/R_e \simeq 1{\cdot}6$) places a lower limit on the density on the eastern edge. This is a lower limit as the radius is more strongly dependent on the density ($R \propto (1/N_0)^{1/4}$) once the momentum-conserving stage is entered, and the part expanding into the denser medium would enter this stage first.

If the density on the western side were sufficiently low, the velocity of expansion could be comparable with the Alfvén velocity and the shock would become weak. This could explain the lack of a shell on the western side of the source. The velocity of expansion of the western half is presumably not less than that of the eastern half, namely 65 km s^{-1}, so for a magnetic field of 3×10^{-6} Gauss, densities of less than 0·1 cm^{-3} would be required for the shock to become weak. This would imply a density to the east of the shell of 1 cm^{-3} and so favour a low energy for the supernova.

4.3. *Physical conditions in the shell*

Van der Laan (1962a) has calculated the enhancement of the background emissivity expected from compression of both the interstellar magnetic field and the relativistic electrons associated with it, and has found that for IC443 with an assumed shell thickness of 5′·2 arc this could account for only one-tenth of the flux at 100 MHz. However, he used very high values for the background emissivity and the distance of IC443. If the shell thickness is taken as 3′ arc van der Laan's theory gives an enhancement of the background emissivity by a factor of 14, and for a shell thickness of 1′ arc, by a factor of 240. At a distance of 1·5 kpc a spherical shell with outer diameter 19′ arc and thickness 3′ arc has a volume $V = 4{\cdot}0 \times 10^{58}$ cm^3. Since the integrated flux from the hemisphere east of a line in position angle 160° through the centre of the shell is $S_{1420} = 105$ f.u., the volume emissivity is $\mathscr{J}_{1420} = 1{\cdot}1 \times 10^{-37}$ W m^{-3} Hz^{-1} sr^{-1}, which is 10^3 times the volume emissivity of the galactic background in this direction as derived from Andrew's (1969) 13 MHz value. This calculation is obviously very approximate but does indicate that if the shell is as thin as 1′ arc this process could contribute significantly to the flux. In the more likely case of a thick shell, this theory cannot explain the radiation from the shell and relativistic electrons generated by the supernova outburst are required (van der Laan 1962b).

There is close agreement between optical and radio emission regions throughout the remnant but, as has been shown in Section 3.4, it is unlikely that this association could be the result of a significant free–free contribution to the radio brightness, particularly in the north-eastern shell. In the western part of the source, and probably also in the north-east, the optical filaments lie along the front edge of the radio features. Spectroscopic observations (Parker 1964) imply a temperature of 10^4°K in the filaments and an average electron density in the filaments, from the [OII] $\lambda3729/\lambda3726$ line ratio, of 350 cm^{-3}. The temperature immediately behind a strong shock moving at 65 km s^{-1} is about 10^5°K, at which temperature radiative cooling is at its most efficient (Heiles 1964; Cox 1970). As the gas cools it is compressed until either an equilibrium temperature of 10^4°K is reached or until the magnetic pressure dominates. The location of the filaments on the leading edge of the shell suggests that they could be part of this cooling region. Poveda (1965) has suggested that the filaments are actually sheets of emission, viewed edge on, in the cooling region behind the shock. If the filaments are in fact contained in the front edge of the compressed region, they must have approximately the same pressure as the gas behind the shock, if they are to be stable. The gas pressure in the filaments is about $N_f kT/\mu = 6 \times 10^{-10}$ erg cm^{-3} where N_f is the electron density in the filaments, T the temperature of the gas in the filaments and $\mu = 0{\cdot}7$ is the molecular weight for the ionized gas. The pressure behind the shock is approximately ρV^2 and if this is to be 6×10^{-10} erg cm^{-3}, an interstellar density of 10 cm^{-3} is required for a shock velocity of 65 km s^{-1}. It has been assumed here that the shock and the shell velocities are the same. This is a good approximation when radiative losses are important and so the compression is high, but for the adiabatic case the shock velocity is a factor of 4/3 greater than the shell velocity and an interstellar density of 5 cm^{-3} would be sufficient to provide a pressure behind the shock equal to that in the filaments. Thus if the filaments are moving with the shell and are in pressure equilibrium with the gas behind the shock, a high interstellar density (> 5 cm^{-3}) is required.

With this density outside the shock and 350 cm^{-3} in the filaments, the gas is compressed by at most a factor of 70 and if the magnetic field in the filaments is the interstellar field compressed with the gas, it is at most a factor of 17 ($=70^{2/3}$) greater than the field outside the shock. The interstellar field would then need to be at least 7×10^{-6} Gauss for the magnetic pressure in the filaments to be important.

Note that the filaments can only occupy a small fraction of the volume of the shell since a shell thickness/radius ratio of one-sixth implies a compression by a factor of only 2·2. The remainder of the shell must be composed of less highly compressed gas at a higher temperature. A second possible origin of the filaments is patches of denser gas which have passed through the shock. Provided they are now moving with the same velocity as the compressed shell this does not alter the density required outside the shock to provide sufficient pressure behind the shock for the filaments to be stable.

The increase in the spectral index at the shell implies a difference in the relativistic electron spectrum. Synchrotron losses cannot produce a break in the radio spectrum below 1·4 GHz with any reasonable value for the compressed field in the shell. A significant contribution to the radiation by enhancement of the background emissivity could only produce a steepening of the spectrum if the shell were thin and the compression were not sufficiently high to displace the break in the galactic background radiation spectrum much above 1·4 GHz. Other possible causes for an increase in the energy spectrum require further investigation.

5. SUMMARY

This high resolution map of IC443 has shown that

(i) The north-eastern shell is thick but probably has a complex structure. This shell is expanding into a region of dense gas if IC443 has an initial energy typical of type II supernovae.

(ii) Optical and radio features are closely related with filaments lying along the outer edges of radio ridges. The high density to the east of the source is consistent with a model of the filaments as areas of highly compressed gas in the cooling region behind the shock.

(iii) The spectral index is high in the vicinity of brightest optical features.

(iv) Only if the density on the east is less than 1 cm^{-3} can the lack of a shell on the western side of the source be explained by the lack of a strong shock on this side.

ACKNOWLEDGMENTS

I am grateful to a number of members of the Radio Astronomy Group for help and advice, in particular Drs J. R. Shakeshaft and D. Downes, and thank I. Rosenberg for providing the model-fitting programme.

I am indebted to the Royal Commission for the Exhibition of 1851, Rhodes University and the C.S.I.R. (South Africa) for awards and support in the period during which this work was carried out.

REFERENCES

Akabane, R., 1966. *Publ. astr. Soc., Japan*, **18**, 96.

Andrew, B. H., 1969. *Mon. Not. R. astr. Soc.*, **143**, 17.

Baldwin, J. E., Jennings, J. E., Shakeshaft, J. R., Warner, P. J., Wilson, D. M. A. & Wright, M. C. H., 1970. *Mon. Not. R. astr. Soc.*, **150**, 253.

Cox, D. P., 1970. Ph.D. Dissert., U. California.
Dickel, J. R., 1971. *Publ. astr. Soc. Pacific.*, **83,** 343.
Erkes, J. W. & Dickel, J. R., 1969. *Astr. J.*, **74,** 840.
Heiles, C., 1964. *Astrophys. J.*, **140,** 470.
Hogg, D. E., 1964. *Astrophys. J.*, **140,** 992.
Kundu, M. R. & Velusamy, T., 1968. *Mon. Not. R. astr. Soc.*, **140,** 173.
Kundu, M. R. & Velusamy, T., 1969. *Astrophys. J.*, **155,** 807.
Locke, J. L., Galt, J. A. & Costain, C. H., 1964. *Astrophys. J.*, **139,** 1071.
Lozinskaya, T. A., 1969. *Astr. Zh.*, **46,** 245, *Sov. Astr.*, **13,** 192.
Milne, D. K., 1971. *Aust. J. Phys.*, **24,** 429.
Milne, D. K. & Hill, E. R., 1969. *Aust. J. Phys.*, **22,** 613.
Minkowski, R., 1968. Chapter 11 of *Nebulae and Interstellar Matter*—eds B. Middlehurst and L. Aller, University of Chicago Press, Chicago.
Minkowski, R., 1971. *The Crab Nebula*, IAU Symposium No. 46, p. 246, D. Reidel Publishing Co. Ltd, Dordrecht, Holland.
Moffat, P. H., 1971. *Mon. Not. R. astr. Soc.*, **153,** 401.
Parker, R. A., 1964. *Astrophys. J.*, **139,** 493.
Poveda, A., 1964. *Ann. Astrophys.*, **27,** 522.
Poveda, A., 1965. *Bol. Obs. Tonantzintla Tacubaya*, **27,** 49.
Poveda, A. & Woltjer, L., 1968. *Astr. J.*, **73,** 65.
Rosenberg, I., 1970. *Mon. Not. R. astr. Soc.*, **147,** 215.
Sedov, L. I., 1959. *Similarity and Dimensional Methods in Mechanics*, Academic Press, New York.
Sharpless, S., 1965. *Galactic Structure*, p. 136, eds A. Blaauw and M. Schmidt, University of Chicago Press, Chicago.
Van der Laan, H., 1962a. *Mon. Not. R. astr. Soc.*, **124,** 127.
Van der Laan, H., 1962b. *Mon. Not. R. astr. Soc.*, **124,** 179.
Woltjer, L., 1970. Chapter 15, in *Interstellar Gas Dynamics*, IAU symposium 39, D. Reidel Publishing Co. Ltd, Dordrecht, Holland.
Wynn-Williams, G., 1969. *Mon. Not. R. astr. Soc.*, **142,** 453.